Performance of an Iris Mechanism Equipped with Fixed and Rotating Deflector Plates for Variable Rate Sprinkler Irrigation

Luiz R. Sobenko[1]; Antonio P. de Camargo[2]; Tarlei A. Botrel[3]; José A. Frizzone[4]; Marcelo F. de Oliveira[5]; Rogério Lavanholi[6]; Jeferson D. M. dos Santos[7]; and Sergio N. Duarte[8]

Abstract: Technologies have been developed for variable rate irrigation (VRI) systems to apply water based on the spatial and temporal variability of field conditions. To verify the suitability of the water distribution patterns of an iris-type mechanism applied in VRI systems, rotating and fixed spray plate sprinklers (RSPSs and FSPSs, respectively) each equipped with two different deflector plates were attached to the mechanism. Tests indoors were performed under the following conditions: iris mechanism orifices 4.93 and 6.94 mm in diameter, a sprinkler at a height of 0.91 m above the ground, and an operating pressure of 103 kPa. Mathematical overlaps were also performed for 1.5,- 2-, and 3-m sprinkler spacing. The results showed that: (1) individual FSPSs distributed water with higher intensity over a smaller distance from the sprinkler than RSPSs, which distributed water at a lower application rate but over a greater distance; (2) the simulated sprinkling uniformities of lateral line travel were 61.2%–91.6% and 88.5%–98.7% for FSPSs and RSPSs, respectively, under different sprinkler spacing conditions; (3) the uniformity of sprinkling decreased by as much as 30.5% for FSPSs and 7.4% for RSPSs with increased sprinkler spacing; (4) FSPSs presented high potential for surface runoff; and (5) the phenomenon of jet inversion did not affect the uniformity of the iris mechanism's water distribution, especially for RSPSs. **DOI: 10.1061/(ASCE)IR.1943-4774.0001431.**

Introduction

Precision agriculture (PA) comprises a set of techniques and methodologies that aim to optimize crop management and the use of agricultural inputs, thus providing maximum economic efficiency and crop production. In this area, technologies focus on the existence of in-field variability, or the site-specific aspects, of natural components, including chemical leaching, runoff, drainage, water content, nutrients, and soil components (Dong et al. 2013). Within the field of PA, one aspect is variable rate irrigation (VRI), studied since the 1990s with a view to identifying when, where, and how much water to apply according to the spatial and temporal variability of field characteristics, such as topography, soil type, water storage capacity, and cropping systems, inter alia, and thus develop appropriate technologies (Stone et al. 2006). In this regard, self-propelled center pivot and linear move sprinkler irrigation systems have been found to be particularly suitable technologies for VRI because of their high level of automation, ease of use, and large area coverage with a single irrigation lateral line (Evans et al. 2012; Kranz et al. 2012).

Commercially available technologies for VRI make it possible to control the amount of water applied in each sector and zone. Focusing on center pivot systems, which currently comprise about 99% of the self-propelled sprinkler market (Evans et al. 2012), the earliest VRI technique was sector control, which used a simple methodology to alter the water application depth through the mechanical adjustment of the speed of lateral travel; this allowed the division of the irrigated area into several pie-slice shaped sectors. In contrast, zone control technologies enable the adjustment of the irrigation depth in each individual sector by changing the discharge rate of sprinklers.

The commercially available mechanism for controlling the flow rate of each sprinkler is based on the duty cycle of a solenoid valve installed at the inlet of each sprinkler, that is, the pulse-width modulation (PWM). However, there are concerns in terms of how the on/off cycles influence the water distribution patterns and uniformity of application of this technology (King and Kincaid 2004; Dukes and Perry 2006). Other methods have been under development to

[1]Ph.D. Student, Dept. of Biosystems Engineering, Univ. of São Paulo, College of Agriculture "Luiz de Queiroz," Piracicaba, SP 13418-900, Brazil (corresponding author). ORCID: https://orcid.org/0000-0002-4958-9149. Email: luizsobenko@usp.br

[2]Professor, Agricultural Engineering College, Univ. of Campinas, Campinas, SP 13083-970, Brazil. ORCID: https://orcid.org/0000-0001-5164-2634. Email: apcpires@unicamp.br

[3]Professor, Dept. of Biosystems Engineering, Univ. of São Paulo, College of Agriculture "Luiz de Queiroz," Piracicaba, SP 13418-900, Brazil. Email: tabotrel@usp.br

[4]Professor, Dept. of Biosystems Engineering, Univ. of São Paulo, College of Agriculture "Luiz de Queiroz," Piracicaba, SP 13418-900, Brazil. Email: frizzone@usp.br

[5]Research Rapid Prototyping, Nucleus of Three-Dimensional Technologies, Renato Archer Information Technology Centre, Campinas, SP 13069-901, Brazil. Email: marcelo.oliveira@cti.gov.br

[6]Ph.D. Student, Dept. of Biosystems Engineering, Univ. of São Paulo, College of Agriculture "Luiz de Queiroz," Piracicaba, SP 13418-900, Brazil. Email: rogeriolavanholi@hotmail.com

[7]Research Mechanical Engineer, Federal Univ. of Paraná, Curitiba, PR 80060, Brazil. Email: jefmotta@hotmail.com

[8]Professor, Dept. of Biosystems Engineering, Univ. of São Paulo, College of Agriculture "Luiz de Queiroz," Piracicaba, SP 13418-900, Brazil. Email: snduarte@usp.br

Note. This manuscript was submitted on December 14, 2018; approved on July 24, 2019; published online on September 18, 2019. Discussion period open until February 18, 2020; separate discussions must be submitted for individual papers. This paper is part of the ***Journal of Irrigation and Drainage Engineering***, © ASCE, ISSN 0733-9437.

address varying application depths along the moving irrigation lateral line. The variable flow sprinkler developed by King and Kincaid (2004) uses a mechanically activated pin to alter the discharge section area, adjusting the sprinkler flow rate based on operating pressure. However, the main concern with this approach is that the wetted pattern and size distribution of the water droplets of the sprinkler change with the flow rate, creating issues for the uniformity of water application with a change in sprinkler pattern overlap.

According to Sourell et al. (2003), the characteristics of spray plate sprinklers, sprinkler spacing, and machine speed will define irrigation performance in all self-propelled sprinkler irrigation systems. Frizzone et al. (2018) also point out that to obtain a more uniform water pattern, sprinklers must be spaced in such a way that each point in the ground receives water from at least three sprinklers. A wide range of sprinkler device types are available in center pivot irrigation systems, from conventional impact sprinklers with different types of nozzles to various types of low-pressure spray plate sprinklers. Impact sprinklers have been replaced by low-pressure spray plate sprinklers, commonly classified as fixed spray plate sprinklers (FSPSs) and rotating spray plate sprinklers (RSPSs), which produce very different droplet size distributions and water application patterns (DeBoer 2002; Faci et al. 2001; Jiao et al. 2017; Sayyadi et al. 2014; Sourell et al. 2003). FSPSs are based on the impact of a water jet on a fixed grooved plate, comprising various numbers or sizes of grooves to break up the water jet into a certain number of small jets that correspond to the number of grooves in the plate. RSPSs can be equipped with different grooved spray plates that rotate under the effect of the water jet, creating momentum on the plate itself; these sprinklers were developed to provide greater jet lengths and lower application rates (Frizzone et al. 2018). Comparing FSPSs and RSPSs, the first type is cheaper and more robust, while the second type presents a more uniform water distribution pattern and greater adaptability to field conditions (Ouazaa et al. 2014).

With the objective of advancing a novel sprinkler concept to be applied in the VRI technique, in a previous work, Sobenko et al. (2018) developed a prototype using an iris-type mechanism actuated by a microstepper motor to vary the discharge section, presenting its complete construction and operating characteristics. This prototype allowed flow rates closer to those required in the field than other means, as well as greater flexibility and accuracy in applying water to the target irrigation depth. However, when the orifice section of the iris mechanism was reduced, the phenomenon of jet inversion occurred, causing the jet to become asymmetrical, which could impair the water distribution patterns. Further investigation of the water distribution patterns was thus required.

Therefore, in this paper an improvement on the prototype previously developed to enable coupling to any commercial sprinkler was reported as an accessory for sprinkler discharge control. The main objective was to verify the water distribution patterns of the prototype coupled to fixed and rotating deflector plates and under discharge adjustments to demonstrate its suitability for variable rate sprinkler irrigation.

Material and Methods

The VRI sprinkler prototype was evaluated in indoor conditions (without wind) at the Irrigation Testing Laboratory (LEMI) of the College of Agriculture "Luiz de Queiroz" (ESALQ/USP), Piracicaba, São Paulo State, Brazil. Its development and operational characteristics are described in full in Sobenko et al. (2018).

Improvements to the Prototype

The structure component of the VRI sprinkler prototype was tailored from the design proposed by Sobenko et al. (2018). The side flaps were replaced by a female ½ in. National pipe thread (NPT) adapter [Item 7.1 in Fig. 1(b)]. With this modification,

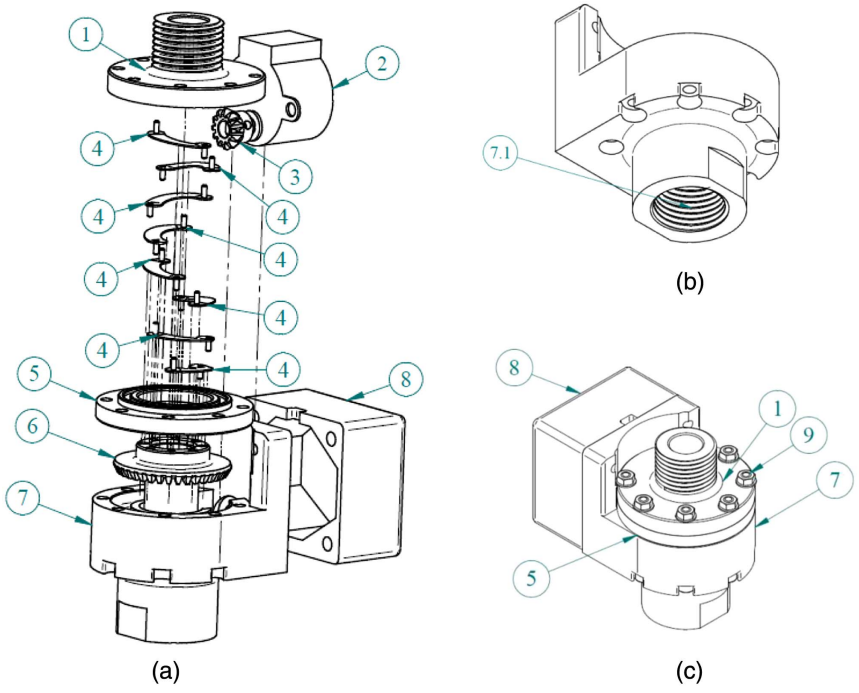

Fig. 1. (a) Detailed view of the improved prototype; (b) new structure component; and (c) assembly. 1 = blade holder; 2 = microstepper motor; 3 = motion/driving gear; 4 = blades; 5 = central body; 6 = driving gear; 7 = structure; 8 = microstepper motor protection; 9 = screws; and 10 = sealing rings.

J. Irrig. Drain Eng., 2019, 145(12): 04019027

Table 1. Manufacturer's specifications of the evaluated sprinklers and deflector plates

Sprinkler	Type	Deflector plate	Number of grooves
Super	Fixed (FSPS)	Flat, no grooves	0
spray		Concave, thick grooves	48
i-Wob	Rotating (RSPS)	Standard angle, small droplet	6
		Standard angle, medium droplet	9

Source: Data from Senninger (2018).

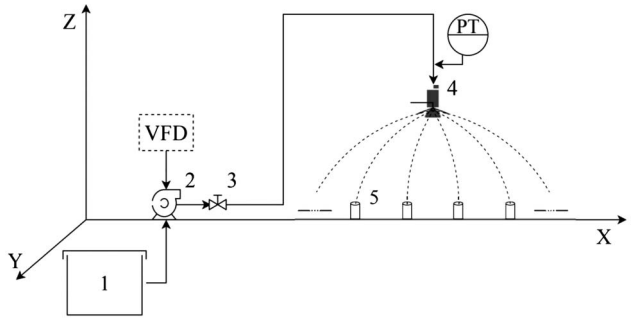

Fig. 2. Instrumentation diagram of the indoor test apparatus. 1 = tank; 2 = pump; 3 = pressure-regulating valve; 4 = sprinkler; and 5 = collectors; VFD = variable frequency driver; and PT = pressure transmitter.

the prototype can be used as an accessory device that can be coupled to commercially available sprinklers to apply water at variable rates (Fig. 1).

The new element was manufactured using Polyjet's additive manufacturing technique at the Three-Dimensional Technologies Laboratory, Renato Archer Information Technology Centre (CTI), Campinas, São Paulo State, Brazil. The Polyjet technique was applied using an acrylic photopolymer jetted via high-resolution inkjet and cured using ultraviolet light, which offers a high surface quality (Esses et al. 2011). The acrylic polymer used was the VeroClear-LGD820 resin in a Connex 350 (Stratasys, Valencia, California) 3D printer, operated in the "digital material" build mode with a layer thickness resolution of 28 μm.

The sprinkler prototype enables adjusting the orifice diameter from 4.9 to 12 mm by using an electronically controlled microstepper motor. Increments in the microstepper motor angle (β), within the range 0°–180°, decrease the orifice diameter according to a quadratic function ($D = -0.00012\beta^2 - 0.02084\beta + 11.33558$, $R^2 = 0.996$). Lower orifice sizes are mechanically possible but would require a stepper motor of higher torque than the one used during the experiments. Since the microstepper motor is electronically controlled, the orifice diameter may assume any value within the aforementioned range and also may be remote adjusted to comply with water requirements at the location being irrigated. The sprinkler may be used both in center pivots and linear move systems.

Conventional Sprinkler Parameters

FSPSs and RSPSs, both from Senninger (Grand Island, Nebraska), were attached to the prototype and each was equipped with two different deflector plates (resulting in four combinations). The parameters of the sprinklers and their corresponding deflector plates are provided in Table 1.

Based on the equation proposed by Sobenko et al. (2018) for predicting the flow through orifices using the variable rate mechanism [Eq. (1)], two orifice sections with diameters of 4.93 (step angle 180°) and 6.94 mm (step angle 126°) were used. The discharge for each configuration was 0.62 and 1.20 $m^3\,h^{-1}$ for step angles of 180° and 126°, respectively, while operating the prototype under 103 kPa (15 psi). These sections of the orifice were selected to verify the water distribution patterns of the sprinkler operating at relatively high and low discharges. Higher values of discharge were not evaluated due to space constraints in terms of carrying out full-grid experiments indoors

$$q = C_d \pi \left\{ [X_3' \sin(\alpha_2')] + \left[\sqrt{r^2 - (r\cos(\alpha_1) - Z_2')^2} - r_1 \right] - B' \right\} \sqrt{2gH} \quad (1)$$

where q = flow rate ($m^3\,s^{-1}$); C_d = discharge coefficient (dimensionless); X_3' = side of the triangle in the iris mechanism, initial condition (m); α_1, α_2' = internal angles of the triangle in the iris mechanism, initial and movement conditions (degrees); r = orifice radius in the iris mechanism, initial condition (m); Z_2' = segment of X_2 in the iris mechanism, movement condition (m); r_1 = segment of orifice radius in the iris mechanism, initial condition (m); B' = blade edge of the iris mechanism in the movement condition (m); g = gravitational acceleration ($m\,s^{-2}$); and H = operation pressure head (m).

Experimental Setup and Water Distribution Measurement Procedure

A structure was mounted in the middle of the experimental plot to determine the application rate and pattern of a single sprinkler (Fig. 2). The prototype was coupled to a rigid pendulum at a height of 0.91 m from the ground, which corresponds to the height described by the sprinkler manufacturer (Senninger 2018). At the inlet of the prototype, a pressure transmitter was connected to monitor the testing pressure, which was set at 103 kPa (15 psi). This operating pressure is commonly found for pressure regulators from several manufacturers (Fabrimar 2018; Nelson 2018; Senninger 2018) and it is used more frequently along a center pivot lateral line (Frizzone et al. 2018). In addition, the other equipment required for pumping and pressure regulation can be seen in Fig. 2.

The water distribution patterns were measured with a series of collectors (Fabrimar, São Paulo, Brazil) arranged in full-grid collector arrays according to the requirements presented by ISO 8026 (ISO 2009). All collectors used in the tests had a height of 80 mm and an opening diameter of 80 mm, which resulted in a collection area of 5.027×10^{-3} m^2. The spacing between the collectors was 0.5 × 0.5 m, arranged in 25 columns × 25 rows (Fig. 3). The values of the eight radii highlighted in Fig. 3 were used to compute the mean radial profile of application. The sprinkler under test was positioned on the middle of the grid, as illustrated in Fig. 3.

The test duration of each experiment was 1 h or less, depending on the application rate and water volume collected by the catch cans. Volumes were measured using graduated cylinders and then converted into water application rates using Eq. (2). Since the sprinkler flow rate was greater than 0.075 $m^3\,h^{-1}$, the effective precipitation rate was assumed to be 0.26 $mm\,h^{-1}$, as recommended by ISO 8026 (ISO 2009). Data from collectors with precipitation rates lower than this value were not computed for distribution pattern determination. Moreover, Table 2 provides detailed information for each test performed

$$h = V\,S^{-1}\,t^{-1} \quad (2)$$

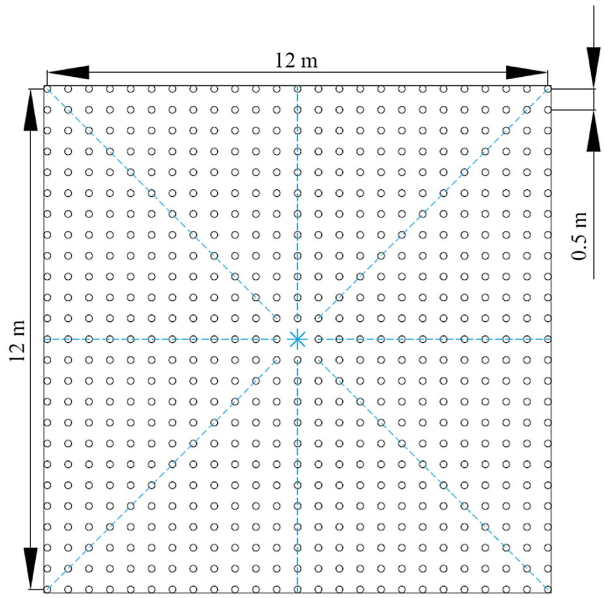

Fig. 3. Collector arrangement for measurements of water distribution.

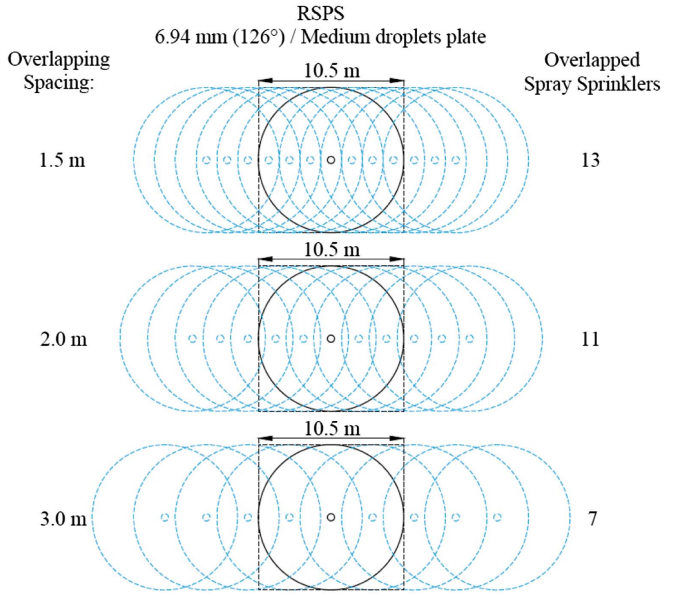

Fig. 4. Schematic example of the mathematical procedure used for simulation of the overlapping of sprinkler spray patterns.

where h = precipitation rate (mm h^{-1}); V = volume collected in each collector (dm^3); S = opening section of the collector (m^2); and t = test duration (h).

Overlap of Sprayers

The data obtained were analyzed and interpolated using the Surfer software (Golden Software, Golden, Colorado). The gridding method used was kriging, with a spacing precision of 0.01 m, which resulted in new matrices of 100 columns × 100 rows.

The individual water distribution matrices obtained for the FSPS and RSPS evaluations were mathematically overlapped to simulate the water application pattern produced by a section of a center pivot or a linear move sprinkler machine. The goal was to obtain a 10.5-m section of fully overlapped water application in the lateral line. Three common values for sprinkler spacing were defined to perform the overlap simulations: 1.5, 2, and 3 m. Installing sprinklers at a single fixed distance along a lateral line facilitates the manufacturing process and the assembling of center pivots or linear move sprinkler machines in the field (Frizzone et al. 2018). The required number of sprinklers used for overlapping varied depending on the spacing and the effective jet length of the sprayer attached to the prototype: 5 (for 3-m spacing), 9 (for 2-m spacing), and 11 (for 1.5-m spacing) for FSPSs; and 7 (for 3-m spacing), 11 (for 2-m spacing), and 13 (for 1.5 m spacing) for RSPSs. Fig. 4 shows an example of the procedure used to overlap the water application for RSPSs equipped with medium droplet plates operating with 6.94-mm orifice diameters. [For further details of the overlapping procedure, see Faci et al. (2001)].

The Christiansen coefficient of uniformity (CUC) was calculated for the fully overlapped section of the lateral using Eq. (3). The CUC simulates the uniformity of the lateral travel of irrigation over a parallel line of the full-grid collector arrays. Although this coefficient is adequate for analyzing the data presented here, and for a linear move system, it is not suitable for the characterization of a complete center pivot lateral due to the increase in the irrigated area produced by each sprinkler toward the end of the lateral line (Faci et al. 2001; Keller and Bliesner 1990)

$$\mathrm{CUC} = \left(1 - \frac{\sum_{i=1}^{n} |h_i - \bar{h}|}{n\,\bar{h}}\right) 100 \tag{3}$$

where CUC = Christiansen coefficient of uniformity (%); h_i = precipitation rate of the i-th observation (mm h^{-1}); $\bar{h}$ = average precipitation rate (mm h^{-1}); and n = number of observations.

In addition, the precipitation rate curves of and irrigation zone irrigated by a set of variable rate sprinklers equipped with FSPSs and RSPSs were simulated and compared to the soil infiltration rate curve to identify risk of surface runoff. For this, as in the procedure for determining the CUC, the fully overlapped section of the lateral obtained by simulating a lateral line of a center pivot traveling over a parallel line of the full-grid collector arrays was used

Table 2. Summary of tests performed with the variable rate prototype

Type	Deflector plate	Orifice diameter (step angle)	Test duration (h)	Flow rate ($m^3\,h^{-1}$)	Operating pressure (kPa)	Installation height (m)
FSPS	Flat	4.93 mm (180°)	0.417	0.62	103	0.91
		6.94 mm (126°)	0.333	1.20	103	0.91
	Concave	4.93 mm (180°)	0.450	0.62	103	0.91
		6.94 mm (126°)	0.333	1.20	103	0.91
RSPS	Small droplet	4.93 mm (180°)	1.000	0.62	103	0.91
		6.94 mm (126°)	0.833	1.20	103	0.91
	Medium droplet	4.93 mm (180°)	0.867	0.62	103	0.91
		6.94 mm (126°)	0.833	1.20	103	0.91

(Faci et al. 2001). Thus, the application rate was computed at each time interval given by the ratio between the new spacing between collectors and the displacement velocity of the last tower. Finally, as the water application profile did not present a symmetrical pattern, the trapezoidal numerical integration rule was used to calculate the applied accumulated depth after the lateral line passage over the irrigated zone. Moreover, for demonstration purposes, the application rates were compared with the infiltration rate presented by Cunha et al. (2015) for the location of Rio Largo, Alagoas, Brazil. The soil in this location is a typical dystrophic cohesive yellow Latosol, characterized by a sandy loam texture and a bulk density of 1,280 kg m^{-3} and cultivated under a minimum tillage system.

Results and Discussion

Water Distribution Patterns of Individual Sprinklers

Fig. 5 represents the wetted patterns generated by the FSPSs [Figs. 5(a–d)] and RSPSs [Figs. 5(e–h)] attached to the prototype. The wetted patterns presented similar profiles despite differences in the magnitude of the application rates. FSPSs applied water at a higher rate closer to the sprinkler and RSPSs distributed water more evenly at a lower application rate and further from the sprinkler (Fig. 5).

The FSPSs tended to distribute most of the water over both sides of the sprinkling axis, while the area around the sprinkling axis received less water, similar to a wetted circular crown, because the deflector plate reduced the velocity of the water and the initial trajectory velocity across the plate was less than the jet velocity (Kincaid 1996). For RSPSs, the application rates declined gradually with increasing distance from the axes. With an increase in orifice diameter, the coverage width of RSPSs increased, the precipitation rates also increased, and the peak of the application rate was further from the sprinkler.

Fig. 6 shows the mean application rate distribution profiles for FSPSs and RSPSs: for the same conventional sprinkler types, the profiles are similar, despite differences in magnitude. By enlarging the orifice section, the location of the higher application rate shifted from around 1.4–2.1 m away from the sprinkler for flat and concave deflector plates [Figs. 6(a and b)]. With an increase in orifice section, the application rate shifted from 2.0 to 2.3 m and from 2.0 to 2.5 m for the small and medium droplet plates, respectively [Figs. 6(c and d)].

For the same sprinkler, the effective wetted radius and wetted area increased as the discharge section increased, that is, with the reduction of the step angle. The wetted radius increased by an average of 25.4% and 18.6% for FSPSs and RSPSs, respectively. The effective wetted area increased by an average of 67.8% for FSPSs and 42.4% for RSPSs (Table 3).

The FSPSs showed peaks of water application clearly visible near the borders of the wetted area, corroborating the results obtained by Faci et al. (2001) and Jiao et al. (2017) when evaluating FSPSs in outdoor conditions and by Sayyadi et al. (2014) when evaluating the same deflector plates indoors. In contrast, the RSPSs presented two peaks of water application, one near the sprinkler outlet and the other at up to 75% of the effective wetted radius. These RSPS distribution profiles were different from those obtained by Faci et al. (2001), Sourell et al. (2003), Playán et al. (2004), and Jiao et al. (2017) when evaluating RSPSs from another manufacturer and at different installation heights.

These differing water distributions between FSPSs and RSPSs were attributable primarily to the different structure of the deflector plates presented in Table 1. The black flat deflector plate used for the FSPS has no grooves, while the blue concave deflector plate has 48 grooves with unique shapes, angles, and depths. However, the deflector plate used for RSPS has grooves with a combination of multiple shapes and depths, including the feature of rotatability, which could generate multiple streams and enable improvement in the water distribution in the presence of diverse soil, plant, and climate conditions.

With regard to existing technologies for applying water at variable rates by changing the discharge section, the prototypes developed by King and Kincaid (2004) and Armindo et al. (2010) both tested RSPSs equipped with four- and six-groove deflector plates. When the prototype developed by King and Kincaid (2004) was tested under similar operating conditions to those used in this work, that is, at a pressure of 138 kPa and an orifice diameter of 4.56 mm, it also resulted in two peaks of water application in its profile, one at approximately 4 m and one of greater intensity near the border of the wetted radius. However, in all tests carried out by Armindo and Botrel (2012), the prototype presented a single peak of water application that was well defined at 4 and 5 m for the four- and six-groove deflector plates, respectively.

Uniformity of Overlapped Water Distribution

The uniformity of water application for a lateral line with sprinklers spaced at 1.5-, 2-, and 3-m intervals was simulated for all of the individual evaluations (Table 4).

The CUC values obtained indicate that the RSPSs presented better water distribution than the FSPSs in all the studied conditions. As the spacing between the sprinklers increased, the CUC values of all sprinklers decreased, especially for the black flat and blue concave deflector plates. The CUC of RSPSs with small droplet deflector plates was less sensitive to an increase in sprinkler spacing, decreasing by only 9.6% and 3.3% for the 4.93-mm and 6.94-mm orifice diameters, respectively. For the 4.93-mm orifice diameter, on average, the FSPSs and RSPSs decreased by 30.5% and 6.7%, respectively. For the 6.94-mm orifice diameter, when the effective wetted area increased, the CUC values were not particularly sensitive to the increase in the sprinkler spacing, decreasing on average by 25.5% and 7.4% for FSPSs and RSPSs, respectively (Table 4).

Jiao et al. (2017) also observed reductions in CUC values with an increase in sprinkler spacing; moreover, with an increase in the discharge section, CUC values tended to decrease slowly relative to increases in sprinkler spacing for FSPSs and RSPSs. Playán et al. (2004) obtained superior CUC values for two RSPSs evaluated in relation to FSPSs, employing the same overlap spacing but increasing the discharge sections and generating an average CUC increase of 22%.

To achieve a uniform water distribution pattern, Frizzone et al. (2018) recommended that the sprinklers should be spaced closely to enable adequate overlap. For FSPSs, this means that the sprinklers must be closer; therefore, a larger number of sprinklers are required, which will result in a higher application rate. Moreover, the wetted circular crown phenomenon previously mentioned for FSPSs became more clearly visible with an increase in orifice diameter and sprinkler spacing. When the sprinkler spacing increased, the continuity of water distribution along the axis of the sprinkler appeared to decrease, presenting as a continuous circular water distribution along the axes, with lower precipitation rates in the middle of the circle and higher precipitation rates at the borders of the circle. For RSPSs, when the sprinkler spacing was increased to 3 m, the continuity of water distribution along the axis of the sprinkler appeared to decrease more smoothly than

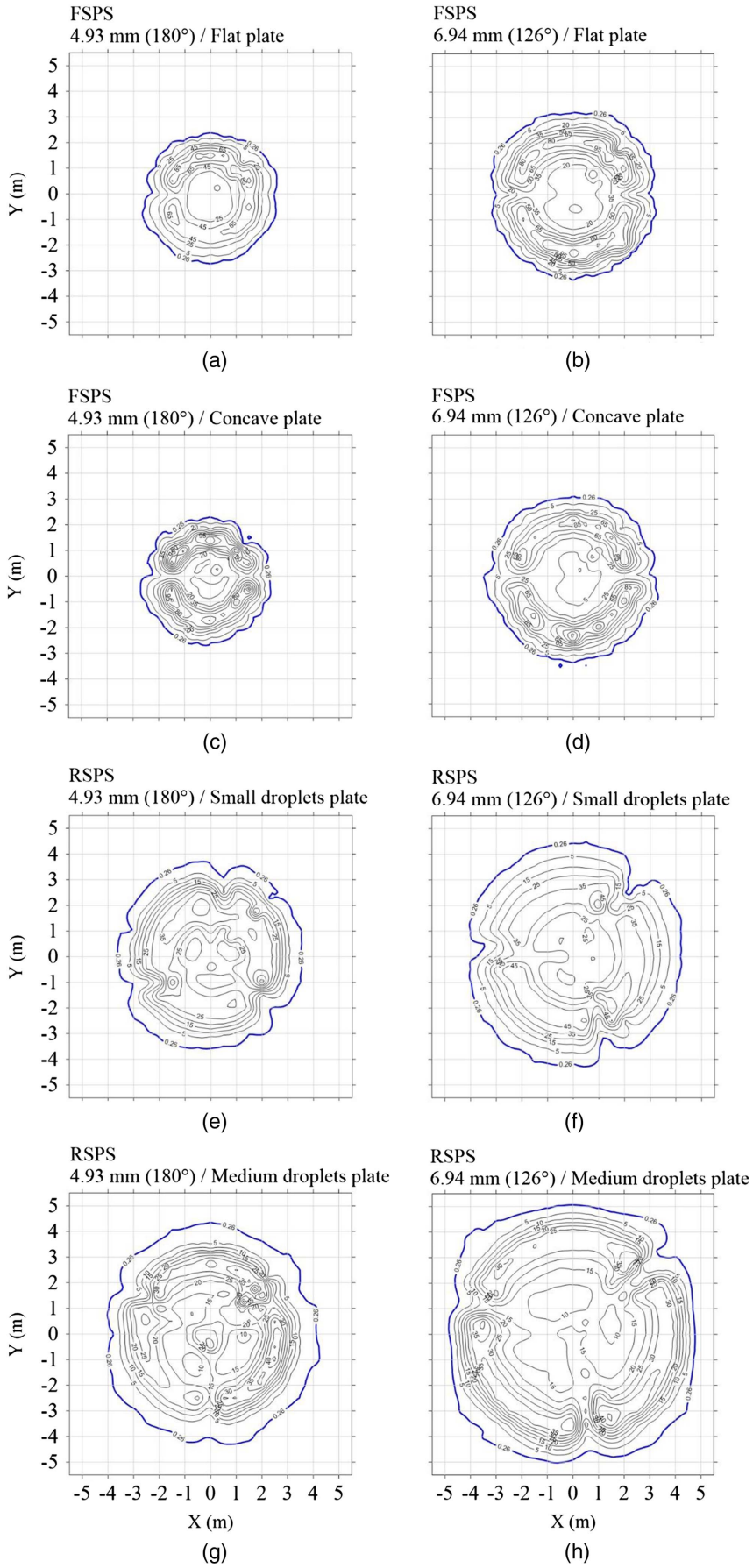

Fig. 5. Wetted patterns (mm h^{-1}) of the prototype operating with two orifice diameters and four different deflector plates.

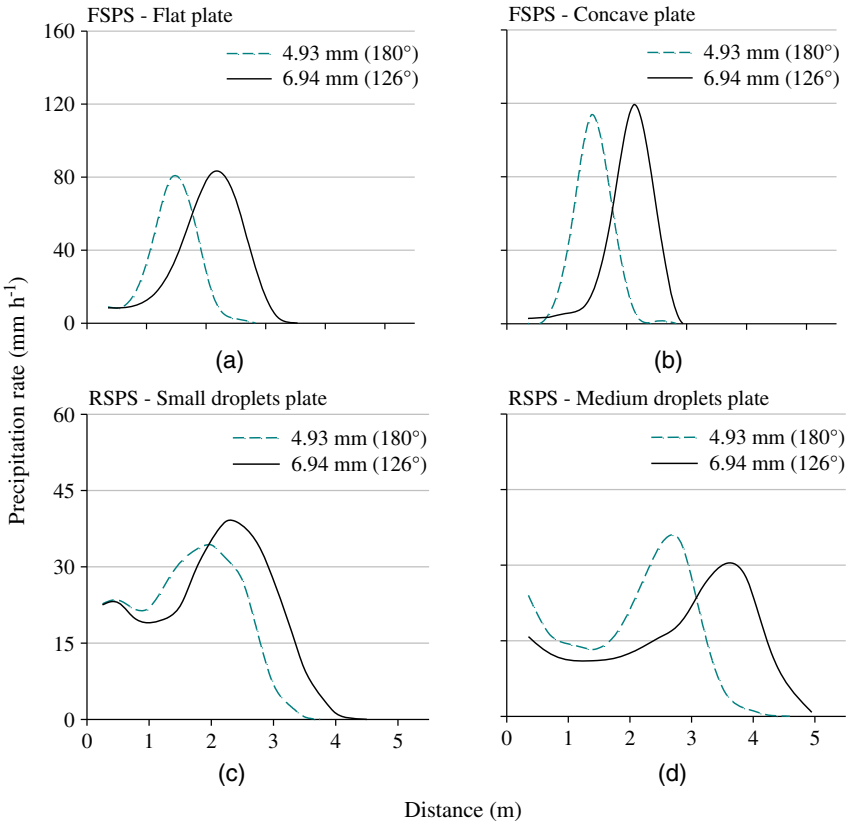

Fig. 6. Mean radial precipitation profiles of the prototype operating with two orifice diameters and four different deflector plates.

Table 3. Observed wetted radii and areas of the prototype operating with two orifice diameters and four different deflector plates

		Orifice diameter (step angle)			
		4.93 mm (180°)	6.94 mm (126°)	4.93 mm (180°)	6.94 mm (126°)
Type	Deflector plate	Wetted radius (m)		Wetted area (m^2)	
FSPS	Flat	2.7	3.3	20.6	33.2
	Concave	2.7	3.5	18.5	32.7
RSPS	Small droplet	3.6	4.2	40.7	56.0
	Medium droplet	4.2	5.1	54.9	80.8

Table 4. Christiansen coefficient of uniformity (CUC) for the variable rate prototype operating with two orifice diameters, four deflector plates, and three sprinkler spacings

		Orifice diameter (step angle)					
		4.93 mm (180°)	6.94 mm (126°)	4.93 mm (180°)	6.94 mm (126°)	4.93 mm (180°)	6.94 mm (126°)
Type	Deflector plate	Spacing 1.5 m		Spacing 2 m		Spacing 3 m	
FSPS	Flat	90.6%	91.4%	82.5%	82.2%	65.3%	68.0%
	Concave	91.6%	89.3%	72.1%	85.7%	61.2%	66.7%
RSPS	Small droplet	97.9%	98.7%	93.6%	97.7%	88.5%	95.4%
	Medium droplet	98.2%	98.5%	95.9%	98.6%	94.3%	87.2%

for FSPSs and the regions of higher and lower precipitation rates alternated along the sprinkling axis. Moreover, based on the CUC values, the phenomenon of jet inversion mentioned by Sobenko et al. (2018) did not appear to impair water distribution uniformity, especially when the prototype was coupled to RSPSs.

Fig. 7 presents an application of the simulated patterns of the precipitation rate versus time for an irrigation lateral line sprinkler equipped with the prototype developed. For this application, a center pivot equipped with variable rate technology irrigating an area of 81.7 ha and operating at a speed equal to 128.7 $m\,h^{-1}$ at the last tower, with a time of revolution of 23 h, was assumed. For comparison purposes, the applied water depth during the wetting time was calculated and an irrigation soil infiltration curve was plotted, considering an irrigation zone in the last tower in which a set of sprinklers may have their orifice diameters adjusted to comply with water requirements at the irrigated zone.

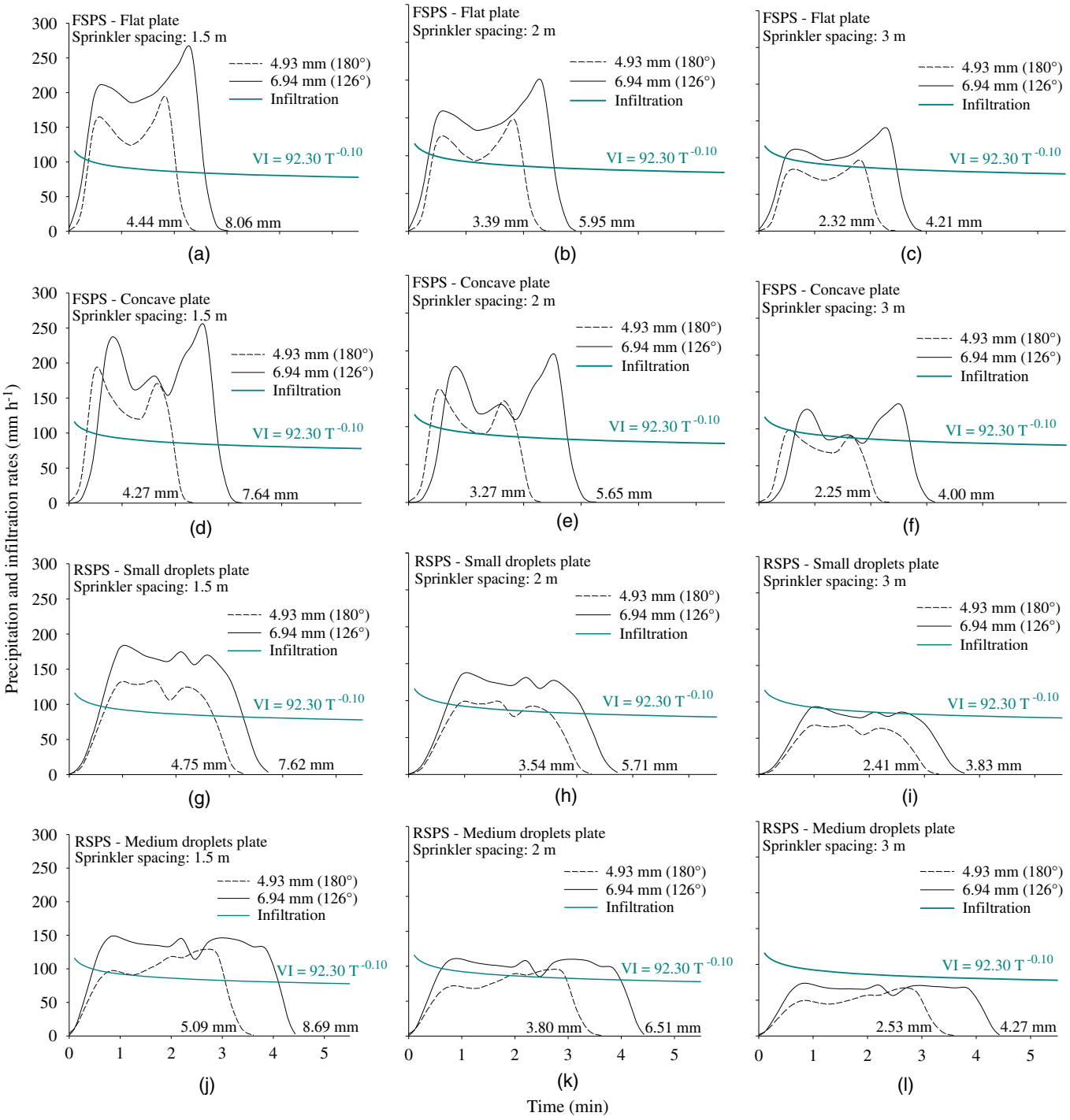

Fig. 7. Precipitation rate versus irrigation time in irrigation lateral equipped with FSPSs and RSPSs with the variable rate prototype operating with different orifice diameters, deflector plates, and sprinkler spacing. Application curves are compared to the soil infiltration rate of Rio Largo, Alagoas, Brazil. Total application depth shown on x-axis at end of precipitation rate curve.

The FSPSs present higher precipitation rates compared to RSPSs with the same nozzle diameters and sprinkler spacing, which could increase the potential for surface runoff and soil erosion (King and Bjorneberg 2011). When the application rate curve exceeds the infiltration velocity curve, surface runoff will occur; this can be quantified as the difference between the irrigation application and the infiltration curve (DeBoer and Chu 2001; Frizzone et al. 2018). Therefore, under the conditions reported here, a high potential for surface runoff for FSPSs with a smaller orifice diameter and spacing can be observed in Figs. 7(a, b, d, and e). Figs. 7(h–l) also indicate the adequacy of the prototype when attached to RSPSs, mainly for larger sprinkler spacings, due to its capability in preventing runoff water losses and other aforementioned characteristics.

Conclusions

The water distribution patterns of the prototype coupled to FSPSs and RSPSs were determined through a set of indoor experiments.

Comparing similar testing conditions for both groups of sprinklers, higher values of CUC, larger wetted areas, and lower application rates and surface runoff potentials were observed for RSPSs. Moreover, RSPSs were less sensitive to increased sprinkler spacing. According to the simulated CUC values, the phenomenon of jet inversion found in an earlier study (Sobenko et al. 2018) apparently did not impair water distribution uniformity, especially when the prototype was coupled to RSPSs, which had sprinkling uniformities of up to 98.7%. In terms of water distribution characteristics, the prototype coupled to FSPSs and RSPSs is suitable for variable rate sprinkler irrigation.

Acknowledgments

This study was financed in part by the Coordenação de Aperfeiçoamento de Pessoal de Nível Superior—Brasil (CAPES)—Finance Code 001.

Notation

The following symbols are used in this paper:

B' = blade edge of the iris mechanism in the movement condition (m);
C_d = discharge coefficient;
CUC = Christiansen coefficient of uniformity (%);
D = orifice diameter (mm);
g = gravitational acceleration, $m\,s^{-2}$;
H = operation pressure head (m);
h = precipitation rate ($mm\,h^{-1}$);
h_i = precipitation rate of the i-th observation ($mm\,h^{-1}$);
$\bar{h}$ = average precipitation rate ($mm\,h^{-1}$);
n = number of observations;
q = flow rate ($m^3\ s^{-1}$);
r = orifice radius in the iris mechanism, initial condition (m);
r_1 = segment of orifice radius in the iris mechanism, initial condition (m);
S = opening section of the collector (m^2);
t = test duration (h);
V = volume collected in each collector (dm^3);
X_3' = side of the triangle in the iris mechanism, initial condition (m);
Z_2' = segment of X_2 in the iris mechanism, movement condition (m);
α_1, α_2' = internal angles of the triangle in the iris mechanism, initial and movement conditions (degrees); and
β = microstepper motor angle (degrees).

References

Armindo, R. A., and T. A. Botrel. 2012. "Performance and radial distribution profiles of a variable flow rate sprinkler developed for precision irrigation." *Sci. Agric.* 69 (2): 160–167. https://doi.org/10.1590/S0103-90162012000200012.

Armindo, R. A., T. A. Botrel, and T. G. Garzella. 2010. "Flow rate sprinkler development for site-specific irrigation." *Irrig. Sci.* 29 (3): 233–240. https://doi.org/10.1007/s00271-010-0231-7.

Cunha, J. L. X. L., M. E. H. Coelho, A. W. Albuquerque, C. A. Silva, A. B. Silva Júnior, and I. D. E. Carvalho. 2015. "Water infiltration curve rate in yellow Latosol under different soil management systems." *Rev. Bras. Eng. Agríc. Ambient.* 19 (11): 1021–1027. https://doi.org/10.1590/1807-1929/agriambi.v19n11p1021-1027.

DeBoer, D. W. 2002. "Drop and energy characteristics of a rotating spray-plate sprinkler." *J. Irrig. Drain. Eng.* 128 (3): 137–146. https://doi.org/10.1061/(ASCE)0733-9437(2002)128:3(137).

DeBoer, D. W., and S. T. Chu. 2001. "Sprinkler technologies, soil infiltration and runoff." *J. Irrig. Drain. Eng.* 127 (4): 234–239. https://doi.org/10.1061/(ASCE)0733-9437(2001)127:4(234).

Dong, X., M. C. Vuran, and S. Irmak. 2013. "Autonomous precision agriculture through integration of wireless underground sensor networks with center pivot irrigation systems." *Ad Hoc Networks* 11 (7): 1975–1987. https://doi.org/10.1016/j.adhoc.2012.06.012.

Dukes, M. D., and C. Perry. 2006. "Uniformity testing of variable-rate center pivot irrigation control systems." *Precis. Agric.* 7 (3): 205–218. https://doi.org/10.1007/s11119-006-9020-y.

Esses, J. S., P. Berman, A. I. Bloom, and J. Sosna. 2011. "Clinical application of physical 3D models derived from MDCT data and created by rapid prototyping." *Am. J. Roentgenol.* 196 (6): W683–W688. https://doi.org/10.2214/AJR.10.5681.

Evans, R. G., J. LaRue, K. C. Stone, and B. A. King. 2012. "Adoption of site-specific variable rate sprinkler irrigation systems." *Irrig. Sci.* 31 (4): 871–887. https://doi.org/10.1007/s00271-012-0365-x.

Fabrimar. 2018. "Performance table." Accessed July 21, 2018. http://www.fabrimar.com.br/categoria?irrigacao=produtos-para-pivo-central.

Faci, J. M., R. Salvador, E. Playán, and H. Sourell. 2001. "Comparison of fixed and rotating spray plate sprinklers." *J. Irrig. Drain. Eng.* 127 (4): 224–233. https://doi.org/10.1061/(ASCE)0733-9437(2001)127:4(224).

Frizzone, J. A., R. Rezende, A. P. Camargo, and A. Colombo. 2018. *Irrigação por aspersão: sistema pivô central*. Maringá, Brazil: Eduem.

ISO. 2009. *Agricultural irrigation equipment: Sprayers: General requirements and test methods*. ISO/DIS 8026. Geneva: ISO.

Jiao, J., Y. Wang, L. Han, and D. Su. 2017. "Comparison of water distribution characteristics for two kinds of sprinklers used for center pivot irrigation systems." *Appl. Sci.* 7 (4): 421. https://doi.org/10.3390/app7040421.

Keller, J., and R. D. Bliesner. 1990. *Sprinkle and trickle irrigation*. New York: Van Nostrand Reinhold.

Kincaid, D. C. 1996. "Spraydrop kinetic energy from irrigation sprinklers." *Trans. ASAE* 39 (3): 847–853. https://doi.org/10.13031/2013.27569.

King, B. A., and D. L. Bjorneberg. 2011. "Evaluation of potential runoff and erosion of four center pivot irrigation sprinklers." *Appl. Eng. Agric.* 27 (1): 75–85. https://doi.org/10.13031/2013.36226.

King, B. A., and D. C. Kincaid. 2004. "A variable flow rate sprinkler for site-specific irrigation management." *Appl. Eng. Agric.* 20 (6): 765–770. https://doi.org/10.13031/2013.17724.

Kranz, W. L., R. G. Evans, F. R. Lamm, S. A. O'Shaughnessy, and R. T. Peters. 2012. "A review of mechanical move sprinkler irrigation control and automation technologies." *Appl. Eng. Agric.* 28 (3): 389–397. https://doi.org/10.13031/2013.41494.

Nelson. 2018. "Irrigation technology for the future: 2018 product catalog." Accessed July 21, 2018. https://nelsonirrigation.com/media/general/2018_CATALOG_NO_LR.pdf.

Ouazaa, S., J. Burguete, M. P. Paniagua, R. Salvador, and N. Zapata. 2014. "Simulating water distribution patterns for fixed spray plate sprinkler using the ballistic theory." *Spanish J. Agric. Res.* 12 (3): 850–863. https://doi.org/10.5424/sjar/2014123-5507.

Playán, E., S. Garrido, J. M. Faci, and A. Galán. 2004. "Characterizing pivot sprinklers using an experimental irrigation machine." *Agric. Water Manage.* 70(3): 177–193. https://doi.org/10.1016/j.agwat.2004.06.004.

Sayyadi, H., A. H. Nazemi, A. A. Sadraddini, and R. Delirhasannia. 2014. "Characterising droplets and precipitation profiles of a fixed spray-plate sprinkler." *Biosyst. Eng.* 119 (Mar): 13–24. https://doi.org/10.1016/j.biosystemseng.2013.12.011.

Senninger. 2018. "Mechanized irrigation: Low pressure-high performance." Accessed July 21, 2018. https://www.senninger.com/sites/senninger.hunterindustries.com/files/senninger-pivot-irrigationproducts-catalog.pdf.

Sobenko, L. R., A. P. Camargo, T. A. Botrel, J. D. M. Santos, J. A. Frizzone, M. F. Oliveira, and L. J. V. Silva. 2018. "An iris mechanism for variable rate sprinkler irrigation." *Biosyst. Eng.* 175 (Nov): 115–123. https://doi.org/10.1016/j.biosystemseng.2018.09.009.

Sourell, H., J. M. Faci, and E. Playán. 2003. "Performance of rotating spray plate sprinklers in indoor experiments." *J. Irrig. Drain. Eng.* 129 (5): 376–380. https://doi.org/10.1061/(ASCE)0733-9437(2003)129:5(376).

Stone, K. C., E. J. Sadler, J. A. Millen, D. E. Evans, and C. R. Camp. 2006. "Water flow rates from a site-specific irrigation system." *Appl. Eng. Agric.* 22 (1): 73–78. https://doi.org/10.13031/2013.20194.